

# Electroweak phase transition in the presence of hypermagnetic field and the generation of gravitational waves

H. Abedi<sup>a 1</sup> M. Ahmadvand<sup>b 2</sup> and S. S. Gousheh<sup>a 3</sup>

<sup>a</sup>*Department of Physics, Shahid Beheshti University, G. C., Evin, Tehran 19839, Iran*

<sup>b</sup>*School of Physics, Institute for Research in Fundamental Sciences (IPM), P. O. Box 19395-5531, Tehran, Iran*

## Abstract

We investigate the effect of a large-scale background hypermagnetic field on the electroweak phase transition. We propose an effective weak angle which is varying during the electroweak phase transition and upon its use, show that for a strong enough hypermagnetic field the phase transition occurs in two steps and becomes first-order. We obtain all of the important quantities characterizing the details of the phase transition, including the phase transition latent heat, temperature and duration. We then explore one of the consequences of this model which is the generation of gravitational waves. We calculate the gravitational wave spectrum generated during the first-order electroweak phase transition and find that, for strong enough background hypermagnetic fields, these signals can be detected by the Ultimate-DECIGO and BBO correlated interferometers.

---

<sup>1</sup>e-mail:hamid\_abedi@sbu.ac.ir

<sup>2</sup>e-mail:ahmadvand@ipm.ir

<sup>3</sup>e-mail:ss-gousheh@sbu.ac.ir

# 1 Introduction

Magnetic fields are ubiquitous in the Universe. The presence of magnetic fields in stars, galaxies and intergalactic spaces raises the question about the origin of these fields [1]. One possibility is that these fields have been produced by some astrophysical and dynamo processes [2]. However, using these mechanisms it is hard to explain large-scale magnetic fields observed in the intergalactic spaces. The other scenario is that these long-range magnetic fields can be relics of the early Universe. In this case, several mechanisms for magnetogenesis have been proposed to be taking place during the early times such as inflation and cosmological phase transitions [3].

Considering such primordial magnetic fields, one can study their effects on significant events taking place after the big bang, e.g. the Electroweak Phase Transition (EWPT). Assuming these magnetic fields are produced before the EWPT, long-range component of these fields, i.e. the hypermagnetic fields, can survive in the plasma with high conductivity. Due to the chiral Abelian anomaly, these hypermagnetic fields can play an important role in the EW baryogenesis scenarios [4, 5]. Furthermore, a background hypermagnetic field,  $B_Y^{\text{bg}}$ , can influence the nature of EWPT. Without such a field, the Standard Model (SM) predicts that the EWPT is a crossover. However, the presence of sufficiently strong hypermagnetic fields could change the situation and make it first-order [6, 7]. On the other hand, due to the coupling between these fields and magnetic dipole moment of sphalerons, the energy barrier of sphalerons decreases so that sphaleron processes can threaten the EW baryogenesis scenarios in this context [8]. In our previous paper [9], based on gravitational anomaly and chiral gravitational waves (GWs) sourced by helical magnetic fields, we found the possibility to violate  $B - L$  symmetry, where  $B$  and  $L$  are baryon and lepton numbers, respectively. Then, relying on sphaleron processes, we presented a possible mechanism for generation of the matter-antimatter asymmetry of the Universe.

The influence of hypermagnetic fields on the EWPT has initially been addressed in [6] and [7]. Considering only the direct effect of hypermagnetic fields on the Gibbs free energy, they showed analytically and also numerically by lattice simulation [10] that the EWPT becomes first-order for strong enough hypermagnetic fields. In this work, starting from an appropriate Lagrangian containing the effect of a constant  $B_Y^{\text{bg}}$  and calculating the effective potential of symmetric and broken phases, we show that by introducing an effective weak angle which is varying during the PT, one can describe the PT dynamically. By analyzing this effective potential we find that as the temperature falls below a temperature  $T_0$ , the vacuum of the symmetric phase becomes unstable and the usual EW crossover transition to a stable vacuum occurs. However, as the temperature decreases further, the presence of a large  $B_Y^{\text{bg}}$  produces a second vacuum whose stability eventually surpasses the first. Consequently, a first-order phase transition occurs between these two well separated vacua. Then, by calculating the bounce solution from the bounce action we find the transition temperature at which the bubbles nucleate. At this temperature, the latent heat of the PT and its relation to the strength of the hypermagnetic fields are obtained. We also calculate the duration of the PT.

A first-order EWPT can have many profound consequences, in particular for matter-antimatter asymmetry generation as well as for the generation of gravitational waves (GWs). Here we concentrate on the latter. The GWs are useful probes, providing valuable information about the early Universe, partly because they have the least attenuation during the propagation. In general, any first-order PT in the early Universe is regarded as a source for the generation of GWs<sup>1</sup> [12, 13]. In this case during the evolution of bubbles three sources can contribute to the production of the GW spectrum: bubble collisions [14], Magnetohydrodynamic (MHD) turbulence [15], and sound waves [16]. In this paper, by calculating the required quantities associated with the PTs, we find the GW energy spectrum. We show that bubbles can run away and the generated GWs can be in the sensitivity range of some future space-based GW experiments, i.e. The Deci-Hertz Interferometer Gravitational Wave Observatory (DECIGO) and the Big Bang Observer (BBO), whose the primary objective is to track primordial GWs [17, 18].

In Section 2, we introduce the one-loop effective action in the presence of an  $B_Y^{\text{bg}}$  and obtain the details of the PT including the bounce solution, transition temperature, duration of the PT and latent heat. In Section 3, we calculate the GWs spectra using the parameters obtained in the previous section. We conclude in Section 4.

## 2 The electroweak phase transition

### 2.1 Model

The presence of a large-scale background hypermagnetic field,  $B_Y^{\text{bg}}$ , at the EWPT, regardless of its origin, can have important consequences on the dynamics on the PT. To study these effects, one can decompose the total hypercharge field strength as  $f_{\mu\nu}^t = f_{\mu\nu} + f_{\mu\nu}^{\text{bg}}$  and consequently the Lagrangian can be written as

$$\mathcal{L} = \mathcal{L}_{SM} - \frac{1}{2}(f^{\text{bg}})_{\mu\nu}f^{\mu\nu} - \frac{1}{4}(f^{\text{bg}})_{\mu\nu}(f^{\text{bg}})^{\mu\nu}, \quad (1)$$

where  $\mathcal{L}_{SM}$  is the Lagrangian of the standard model. As shown in [7], one can solve the equations of motion for both symmetric and broken phases and then obtain the corresponding Gibbs free energies in terms of  $B_Y^{\text{bg}}$ . In the high conductive plasma of the symmetric phase, only the large-scale hypermagnetic field can survive while other fields are screened. Moreover, in the case of a first-order PT and existing of bubbles, in order for the Z-component not to penetrate the bubbles, the wall width should be larger than the correlation length of the field, i.e.  $l_{\text{wall}} > l_Z$ . Only the Maxwellian component of  $B_Y^{\text{bg}}$  remains unscreened. Also, there is a criterion to avoid the W-condensation, i.e.  $eB_Y^{\text{bg}} < (m_W\phi/v)^2$  [7]. We will investigate these constraints in the next section.

The Gibbs free energies corresponding to the effective potentials in the symmetric and broken phases are given by  $V(0, T)$  and  $V(\phi, T) + 1/2(B_Y^{\text{bg}})^2 \sin^2 \theta_w$ , respectively. Here

---

<sup>1</sup>The relation of hypermagnetic fields to the GW radiation at the EWPT is initiated in [11]

$\theta_w$  is the Weinberg or weak mixing angle. These free energies correspond to those of [7] which have been shifted by  $1/2(B_Y^{\text{bg}})^2$  due to the last term of Eq. (1), although the physics of the system will be unchanged. Similar to the Meissner effect, one can study effects of the extra energy difference between two phases,  $1/2(B_Y^{\text{bg}})^2 \sin^2 \theta_w$ , by a single form effective potential. To obtain this potential, one can consider an effective weak angle which varies during the EWPT from zero in the symmetric phase to its final nonzero value, i.e.,  $\theta_w$ , in the broken phase. An analogous scheme for the weak angle varying with time has been studied in [19]. Since the Higgs VEV varies with temperature, we propose a phenomenological Ansatz for the weak effective angle as below,

$$\Theta_w = \theta_w \left[ \frac{1}{2} + \frac{1}{2} \tanh \left( \frac{\phi - m}{s} \right) \right], \quad (2)$$

where  $m$  and  $s$  are two constants which determine the mid-value of  $\phi$  and the smoothness of  $\Theta_w$  profile, respectively. Consequently, we use the following potential as the finite temperature effective potential which describes the system during the phase transition and is valid in the symmetric and broken phases

$$V_{eff}(\phi, T, B_Y^{\text{bg}}) = V(\phi, T) + \frac{(B_Y^{\text{bg}})^2}{2} \sin^2 \Theta_w. \quad (3)$$

The phenomenological Ansatz we have chosen for  $\Theta_w(\phi)$  is a natural smooth choice consistent with mentioned requirements. As a result, our proposed effective potential coincides with the corresponding Gibbs free energies in the symmetric and broken phases, and can describe the dynamics of the PT continuously.

In Fig. (1),  $\Theta_w$  is shown for  $m = 95$  and  $s = 10$ . These parameters are chosen in such a way as to not only avoid the Z-penetration of the bubbles and W-condensation, but also make baryogenesis possible<sup>2</sup>. Conductivity of primordial plasma is proportional to its temperature [10], and hence is very high. In such a plasma, the only long-range or background field that can survive is  $B_Y^{\text{bg}}$ . We assume such long-range  $B_Y^{\text{bg}}$  exist and that their scale is much larger than the typical size of bubbles during the PT. Therefore we take this field to be constant on the scale of the bubbles and further assume  $B_Y^{\text{bg}} = bT^2$  where  $b$  is approximately constant during the EWPT.

In Eq. (3),  $V(\phi, T)$  consists of the following terms

$$V(\phi, T) = V_0 + V_1 + V_{th}, \quad (4)$$

where the tree level potential of the Higgs field,  $V_0$ , is given by

$$V_0(\phi) = -\frac{1}{2}\mu^2\phi^2 + \frac{\lambda}{4}\phi^4, \quad (5)$$

where  $\lambda = \mu^2/\nu^2$  is fixed by the Higgs mass,  $2\lambda\nu^2 = 125 \text{ GeV}$ , and Higgs VEV at zero temperature,  $\nu = 246 \text{ GeV}$ . One-loop quantum correction can be written as [20]

---

<sup>2</sup>In order for the sphalerons to be active outside the bubbles before the transition temperature,  $v(T)/T$  must be sufficiently less than one. This condition can be satisfied for  $m < 100$ . On the other hand, as for avoiding W-condensation,  $m > 90$  is acceptable. Hence, considering these two constraints, we can take  $90 < m < 100$ .

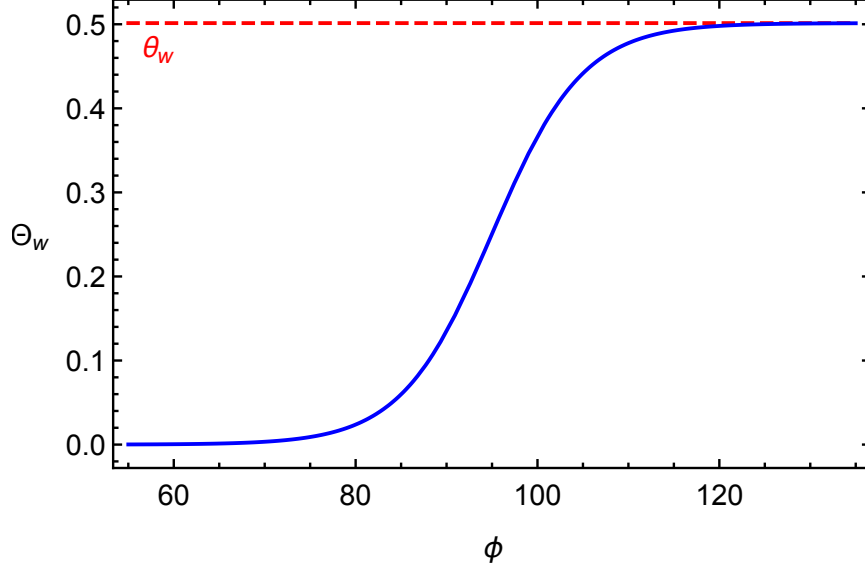


Figure 1: Our proposed model for the weak angle as a function of  $\phi$  during the EWPT for  $m = 95$  and  $s = 10$ .

$$\begin{aligned}
V_1(\phi) &= \frac{6}{64\pi^2} \left[ m_W^4(\phi) \left( \log \frac{m_W^2(\phi)}{m_W^2(\nu)} - \frac{5}{6} \right) + 2m_W^2(\phi)m_W^2(\nu) \right] \\
&+ \frac{3}{64\pi^2} \left[ m_Z^4(\phi) \left( \log \frac{m_Z^2(\phi)}{m_Z^2(\nu)} - \frac{5}{6} \right) + 2m_Z^2(\phi)m_Z^2(\nu) \right] \\
&- \frac{12}{64\pi^2} \left[ m_t^4(\phi) \left( \log \frac{m_t^2(\phi)}{m_t^2(\nu)} - \frac{3}{2} \right) + 2m_t^2(\phi)m_t^2(\nu) \right], \tag{6}
\end{aligned}$$

where  $m_W(\phi) = g_2\phi/2$ ,  $m_Z(\phi) = \sqrt{(g_2^2 + g'^2)}\phi/2$  and  $m_t(\phi) = y_t\phi/\sqrt{2}$  are masses of the massive gauge fields and the top quark, respectively. The thermal correction term is as follows [20]

$$V_{th}(\phi, T) \equiv \sum_{i=W,Z,t} \pm \frac{n_i T^4}{2\pi^2} J_{B,F} \left( \frac{m_i^2(\phi)}{T^2} \right), \tag{7}$$

where  $n_i$  is the number of degrees of freedom of the mentioned particles and

$$J_{B,F}(x) = \int_0^\infty dy y^2 \log \left[ 1 \mp \exp \left( -\sqrt{y^2 + x} \right) \right]. \tag{8}$$

High temperature expansion of the thermal corrections is as follows

$$J_B(x) = \frac{\pi^2}{12}x - \frac{\pi}{6}x^{\frac{3}{2}} - \frac{x^2}{32} \log \frac{x}{a_b} + \mathcal{O}(x^3), \tag{9}$$

$$J_F(x) = -\frac{\pi^2}{24}x - \frac{x^2}{32} \log \frac{x}{a_f} + \mathcal{O}(x^3), \quad (10)$$

where  $\log a_b = 5.4076$  and  $\log a_f = 2.6351$ . In the next subsection, within the above model, we calculate all of the major physical quantities characterizing the phase transition.

## 2.2 Dynamics of the phase transition

In a typical PT, the existence of a barrier between two minima of the effective potential produces a first-order PT. In [6, 7], using only the difference of the Gibbs free energies of two phases and without considering the PT dynamics, it is argued that the presence of a strong enough  $B_Y^{\text{bg}}$  in the effective potential increases the area under the barrier and delays the PT<sup>2</sup>. In this paper, we use  $V_{eff}$  as given by Eqs. (3, 2) to calculate the dynamics of the EWPT. In Fig. (2) we plot  $V_{eff}$  as a function of  $\phi$  for a few important temperatures, all at a fixed value of  $B_Y^{\text{bg}}$ . In the symmetric phase and well above the EWPT the system has a stable vacuum at  $\phi = 0$ . As the temperature decreases to  $T_0 \approx 163$  GeV, the second derivative at  $\phi = 0$  becomes zero and the vacuum becomes metastable. As the temperature decreases further, a stable minimum starts to form and the VEV continuously increases from zero through the usual EW crossover. The new feature in the presence of a strong  $B_Y^{\text{bg}}$  is the formation of a second minimum, when the temperature decreases further. At the critical temperature,  $T_c$ , the two vacua become degenerate. Shortly after  $T_c$ , at nucleation or transition temperature,  $T_*$ , the newly formed vacuum becomes the absolute minimum and tunneling to the true vacuum can be fulfilled. Finally, at temperature  $T_f \approx 118$  GeV the barrier between the minima disappears, i.e. only one vacuum remains. This temperature can be considered as the end of the EWPT.

The probability of true vacuum bubble nucleation per unit Hubble spacetime volume at finite temperature is given by [21]

$$P \simeq \frac{M_{\text{pl}}^4}{T^4} \exp\left(-\frac{S_3(T)}{T}\right), \quad (11)$$

where  $M_{\text{pl}}$  is the Planck mass and  $S_3(T)$  is the three-dimensional Euclidean bounce action<sup>3</sup>

$$S_3(T) = \int_0^\infty 4\pi r^2 dr \left[ \frac{1}{2} \left( \frac{d\phi}{dr} \right)^2 + V_{eff}(\phi, T, B_Y^{\text{bg}}) \right]. \quad (12)$$

As shown below, the presence of a strong hypermagnetic field can significantly affect the bounce action, and in particular the EWPT is delayed. In fact, the transition

---

<sup>2</sup>It should be noted that in [6, 7] the value of  $B_Y^{\text{bg}}$  required for the strongly first-order EWPT is calculated before the observation of the Higgs particle.

<sup>3</sup>It should also be noted that the hypermagnetic field may deform the bubbles and degrade the spherical symmetry to an axial symmetry. Therefore the calculations presented are an approximation. An attempt to improve the calculations should include the back-reaction of the plasma which might produce a restoring force.

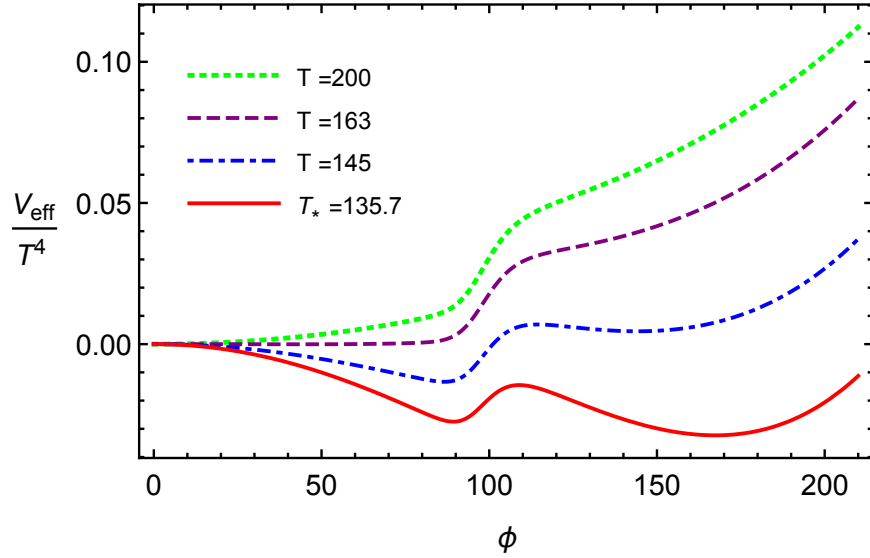


Figure 2: The effective potential at different temperatures for  $B_Y^{\text{bg}} = 0.5 T_*^2$  is displayed. The green dotted curve is at  $T = 200$  GeV far above the PT with one minimum at  $\phi = 0$ , the purple dashed curve at  $T_0 = 163$  GeV shows the beginning of crossover, the blue dotdashed curve  $T = 145$  GeV depicts a typical case where the second local minimum is forming, and the red solid curve corresponds to the nucleation temperature  $T_* = 135.7$  GeV. Since  $T_c = 137.2$  GeV is very close to  $T_*$ , we do not show its curve. Also not shown is the curve for  $T_f \approx 118$  GeV, where only one minimum remains.

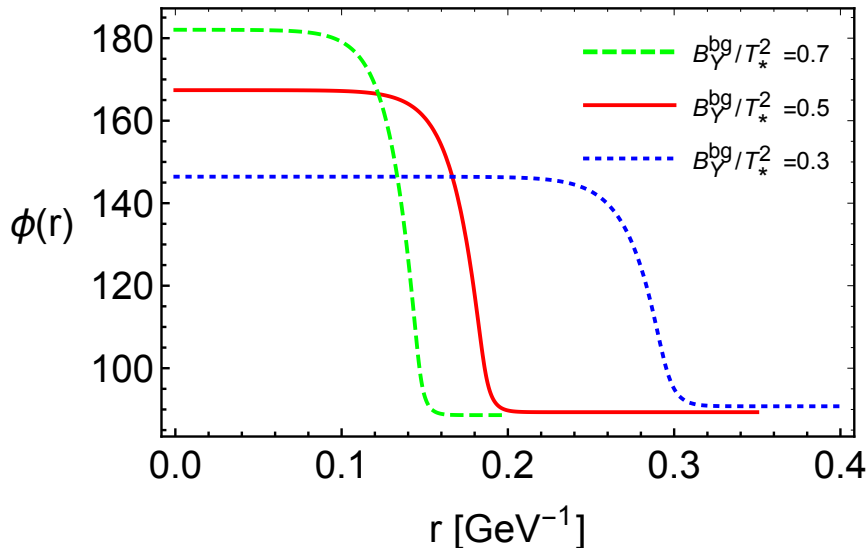


Figure 3: The Higgs bubble profile or the bounce solution that separates the two phases is shown for three different values of  $B_Y^{\text{bg}}$ .

and bubble nucleation occurs when the bubble formation probability is of the order of one,  $P \sim 1$ . From this condition, we can find the transition temperature,  $T_*$ , [21]

$$\frac{S_3(T_*)}{T_*} = 4 \ln \left( \frac{T_*}{H_*} \right), \quad (13)$$

where  $H \simeq T^2/M_{\text{pl}}$  is the Hubble expansion parameter. Thus, we should first obtain the function  $S_3(T)/T$ . Extremizing the bounce action leads to the bounce equation which is shown below along with the appropriate boundary conditions,

$$\frac{d^2\phi}{dr^2} + \frac{2}{r} \frac{d\phi}{dr} = \frac{\partial V_{\text{eff}}}{\partial \phi}, \quad \frac{d\phi}{dr}(r=0) = 0, \quad \phi(r=\infty) = \phi_{\text{false}}. \quad (14)$$

From these equations, we can find the radial profile of the Higgs, i.e. the bounce solution, which, as we shall see, connects the two phases through a step-like but smooth function. To obtain the solution, we use the “any bubble” code [22] which takes advantage of a multiple-shooting method. The result is shown in Fig. (3). The expectation value of the Higgs field inside the bubble is completely consistent with the absolute minimum of the red solid curve in Fig. (2). Moreover, as shown in Fig. (3), the wall width of the true vacuum bubbles,  $l_w \sim (0.04-0.06) \text{ GeV}^{-1}$ , is larger than the correlation length of Z-field,  $l_Z \sim 1/m_Z = 2/(\sqrt{g_2^2 + g'^2}v(T_*)) \sim 0.01 - 0.02 \text{ GeV}^{-1}$ , which is compatible with our assumptions.<sup>4</sup>

Putting the bounce solution into the Eq. (12) and computing the integral, we obtain  $S_3(T)/T$  as a function of temperature. Then, using Eq. (13), we calculate

<sup>4</sup>To prevent the W-condensation at the transition temperature,  $eB_Y^{\text{bg}} < g_2^2 v(T_*)^2/4$  which sets an upper bound for the values of  $B_Y^{\text{bg}}$  that we study in this paper.



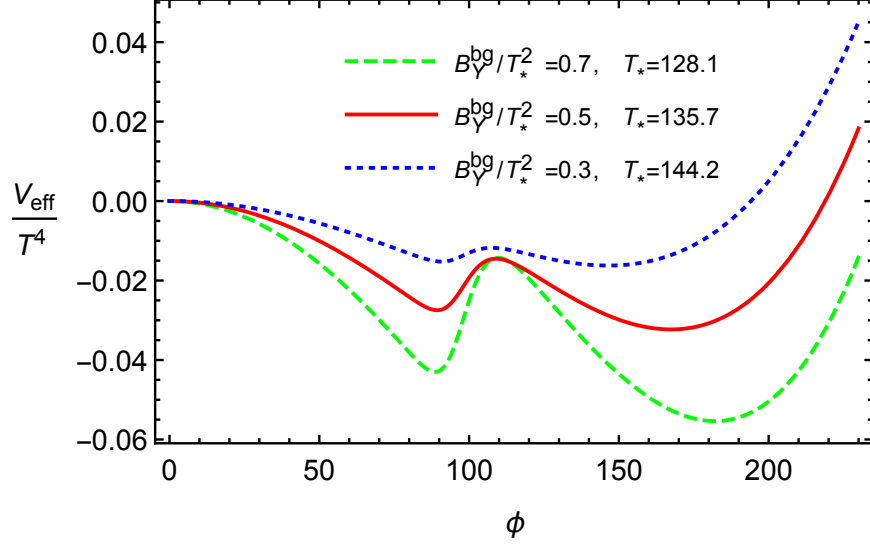


Figure 4: The effective potential is shown at transition temperature for various values of the background hypermagnetic field.

the transition temperature,  $T_*$ , for different hypermagnetic field values and show the results in Fig. (4). As seen from Fig. (4), by increasing  $B_Y^{\text{bg}}$ , the barrier between the vacua is increased and PT occurs at a lower temperature.

Other important PT characteristics such as latent heat and duration of the PT are computed at  $T_*$ . The latent heat is given by

$$L = -T_c \left. \frac{d\Delta V_{eff}(T)}{dT} \right|_{T_c}, \quad (15)$$

from which one can define the vacuum energy density as

$$\epsilon_* = \left( \Delta V_{eff}(T) - T \frac{d\Delta V_{eff}(T)}{dT} \right) \Big|_{T=T_*}, \quad (16)$$

where  $\Delta V_{eff}(T_*) = V_{eff}(\phi_{\text{false}}(T_*), T_*) - V_{eff}(\nu(T_*), T_*)$ . Moreover, the duration of the PT,  $\tau^{-1}$ , can be obtained by the following procedure. We assume bubbles nucleate with a rate per spacetime volume which is given by<sup>5</sup>  $P = P_0 \exp(\tau t)$ . As a result, we have  $\tau = \dot{P}/P$ . Then, according to  $dT/dt \simeq -HT$  and Eq. (11), we can find  $\tau$  from  $S_3(T)/T$  function at  $T_*$  obtained in the previous section [23]

$$\frac{\tau}{H_*} = T_* \frac{d}{dT} \left( \frac{S_3(T)}{T} \right) \Big|_{T_*}. \quad (17)$$

<sup>5</sup>Here we adhere to the usual definition, with the understanding that  $t$  terminates at  $t_*$  corresponding to  $T_*$ .

| $B_Y^{\text{bg}}/T^2$ | $T_c[\text{GeV}]$ | $T_*[\text{GeV}]$ | $S_3(T_*)/T_*$ | $L[\text{GeV}^4]$  | $\epsilon_*[\text{GeV}^4]$ | $\tau/H_*$        |
|-----------------------|-------------------|-------------------|----------------|--------------------|----------------------------|-------------------|
| 0.3                   | 144.8             | 144.2             | 144.5          | $1.02 \times 10^8$ | $1.02 \times 10^8$         | $6.6 \times 10^4$ |
| 0.5                   | 137.2             | 138.9             | 144.8          | $1.51 \times 10^8$ | $1.50 \times 10^8$         | $2.5 \times 10^4$ |
| 0.7                   | 130.4             | 128.1             | 145.0          | $1.87 \times 10^8$ | $1.84 \times 10^8$         | $1.5 \times 10^4$ |

Table 1: The values of the critical temperature, the transition temperature, the on-shell bounce action, the latent heat, the vacuum energy density and the inverse of PT duration are shown for three different values of  $B_Y^{\text{bg}}$ .

In Table 1, we show values of various quantities characterizing the EWPT, including  $\epsilon_*$  and  $\tau$ , for three values of  $B_Y^{\text{bg}}$ . It is interesting to note that  $\tau^{-1} \sim 10^{-3}(t_f - t_*)$ , where  $t_f$  and  $t_*$  are the times associated with  $T_f$  and  $T_*$ , respectively. In the next section, we will use these quantities for computing the spectrum of the GWs produced during the EWPT.

### 3 Gravitational wave generation

In this section, we calculate the spectrum of the GW generated during the first-order EWPT. Considering the ever increasing detection capabilities of GW detectors, GW can be used as an effective probe of the early Universe. In particular, we investigate whether the GW produced in our model falls within the detection range of Ultimate-DECIGO and BBO correlated interferometers.

During cosmological first-order PTs and evolution of the bubbles of true vacuum, three processes can give rise to GW radiation. Indeed, when bubbles nucleate and grow, because of their collisions, part of the latent heat released during the transition is converted to GWs. Moreover, a fraction of the energy is transferred to the plasma and causes the plasma motion which in turn puts forward two other GW sources: MHD turbulence and sound waves.

The contribution of the first mentioned source to the GW frequency spectrum is calculated by numerical simulations using the envelope approximation and expressed in terms of the PT parameters [23]:

$$h^2 \Omega_{en}(f) = 1.67 \times 10^{-5} \left( \frac{0.11 v_b^3}{0.42 + v_b^2} \right) \left( \frac{H_*}{\tau} \right)^2 \left( \frac{\kappa \alpha}{1 + \alpha} \right)^2 \left( \frac{100}{g_*} \right)^{\frac{1}{3}} S_{en}(f), \quad (18)$$

where  $h$  is the present Hubble parameter  $H_0$  in units of  $100 \text{ km sec}^{-1} \text{ Mpc}^{-1}$ ,  $v_b$  is the bubble wall velocity, the factor  $\kappa$  stands for the fraction of the vacuum energy which is converted into the kinetic energy of the bubbles,  $g_* \simeq 106$  is the number of effective relativistic degrees of freedom at the EWPT and  $\alpha$  denotes the ratio of the vacuum energy density to the thermal energy density

$$\alpha = \frac{\epsilon_*}{\frac{\pi^2}{30} g_* T_*^4}. \quad (19)$$

The Expression for  $\epsilon_*$  is given by Eq. (16). The spectral shape of the GW is given by the following analytic fit [24]

$$S_{en}(f) = \frac{3.8\left(\frac{f}{f_{en}}\right)^{2.8}}{1 + 2.8\left(\frac{f}{f_{en}}\right)^{3.8}}, \quad (20)$$

where the present-day red-shifted peak frequency is given by the following relation

$$f_{en} = 16.5 \times 10^{-6} \left( \frac{0.62}{1.8 - 0.1v_b + v_b^2} \right) \left( \frac{\tau}{H_*} \right) \left( \frac{T_*}{100 \text{ GeV}} \right) \left( \frac{g_*}{100} \right)^{\frac{1}{6}}. \quad (21)$$

Furthermore, we should take into account the other two sources contributing to the GW energy density. Gravitational wave contributions from sound waves, which is numerically calculated in [25], and MHD turbulence as a Kolmogorov-type turbulence modeled by [26] are given by

$$h^2\Omega_{sw}(f) = 2.65 \times 10^{-6} \left( \frac{H_*}{\tau} \right) \left( \frac{\kappa_{sw}\alpha}{1 + \alpha} \right)^2 \left( \frac{100}{g_*} \right)^{\frac{1}{3}} v_b S_{sw}(f), \quad (22)$$

and

$$h^2\Omega_{tu}(f) = 3.35 \times 10^{-4} \left( \frac{H_*}{\tau} \right) \left( \frac{\kappa_{tu}\alpha}{1 + \alpha} \right)^{\frac{3}{2}} \left( \frac{100}{g_*} \right)^{\frac{1}{3}} v_b S_{tu}(f), \quad (23)$$

where their spectral shapes are as follows [27]

$$S_{sw}(f) = \left( \frac{f}{f_{sw}} \right)^3 \left( \frac{7}{4 + 3\left(\frac{f}{f_{sw}}\right)^2} \right)^{\frac{7}{2}}, \quad (24)$$

$$S_{tu}(f) = \frac{\left(\frac{f}{f_{tu}}\right)^3}{\left(1 + \frac{f}{f_{tu}}\right)^{\frac{11}{3}} \left(1 + \frac{8\pi f}{h_*}\right)}, \quad (25)$$

with

$$h_* = 16.5 \times 10^{-6} [\text{Hz}] \left( \frac{T_*}{100 \text{ GeV}} \right) \left( \frac{g_*}{100} \right)^{\frac{1}{6}}, \quad (26)$$

as the red-shifted Hubble parameter. The red-shifted peak frequencies in the spectral shapes of these GW spectra are given by

$$\begin{aligned} f_{sw} &= 1.9 \times 10^{-5} \left( \frac{1}{v_b} \right) \left( \frac{\tau}{H_*} \right) \left( \frac{T_*}{100 \text{ GeV}} \right) \left( \frac{g_*}{100} \right)^{\frac{1}{6}}, \\ f_{tu} &= 2.7 \times 10^{-5} \left( \frac{1}{v_b} \right) \left( \frac{\tau}{H_*} \right) \left( \frac{T_*}{100 \text{ GeV}} \right) \left( \frac{g_*}{100} \right)^{\frac{1}{6}}. \end{aligned} \quad (27)$$

As can be easily seen from Eqs. (18-27), the bubble growth velocity,  $v_b$ , has an important role in the frequency distribution of GWs originating from each of the three sources. An important parameter which affects  $v_b$  is  $\alpha$  as defined in Eq. (19). In particular, a critical value of  $\alpha$  is given by [27]

$$\alpha_\infty = \frac{30}{24\pi^2} \frac{\sum_i c_i \Delta m_i^2(\phi_*)}{g_* T_*^2}, \quad (28)$$

| $B_Y^{\text{bg}}/T_*^2$ | $\alpha$ | $\alpha_\infty$ |
|-------------------------|----------|-----------------|
| 0.3                     | 0.007    | 0.003           |
| 0.5                     | 0.013    | 0.005           |
| 0.7                     | 0.020    | 0.008           |

Table 2: For three different values of  $B_Y^{\text{bg}}$ ,  $\alpha$  and  $\alpha_\infty$  which are necessary to specify GW signals are displayed.

where  $c_i = n_i$  ( $c_i = n_i/2$ ) and  $n_i$  is the number of degrees of freedom for boson (fermion) species and  $\Delta m_i^2$  is the squared mass difference of particles between two phases. Thus, the main contribution to  $\alpha_\infty$  comes from the particles becoming heavy during the PT, i.e.  $W$ ,  $Z$  gauge bosons and  $t$  quark. For  $\alpha < \alpha_\infty$ ,  $v_b$  remains subluminal and the available energy is transformed into fluid motion. hence the dominant contributions to GW come from sound waves and MHD turbulence, i.e.  $h^2\Omega(f) \simeq h^2\Omega_{sw} + h^2\Omega_{tu}$ .

For  $\alpha > \alpha_\infty$  the bubbles are “runaway”, that is the excess vacuum energy density leads to bubble acceleration and  $v_b$  is bounded only by the speed of light,  $v_b = 1$ . In this case, all three sources contribute to the GW spectrum, i.e.  $h^2\Omega(f) \simeq h^2\Omega_{en} + h^2\Omega_{sw} + h^2\Omega_{tu}$ .

In Table 2, we show values of  $\alpha$  and  $\alpha_\infty$  for three different values of  $B_Y^{\text{bg}}$ . In all of these cases  $\alpha > \alpha_\infty$  so that bubbles are runaway, i.e.  $v_b = 1$ . In this case, the efficiency factor for the bubble collision source, which enters directly in Eq. (18), can be expressed as [27, 28]

$$\kappa = 1 - \frac{\alpha_\infty}{\alpha}. \quad (29)$$

In fact the fraction  $\alpha_\infty/\alpha$  is transformed into the fluid motion and thermal energy. A fraction  $\kappa_\infty$  of  $\alpha_\infty/\alpha$  is converted to the plasma motion with the efficiency factor  $\kappa_v$ , and the remaining is spent for reheating the plasma by the efficiency factor  $\kappa_{th}$  [27, 28],

$$\kappa_v = \frac{\alpha_\infty}{\alpha} \kappa_\infty, \quad \kappa_{th} = \frac{\alpha_\infty}{\alpha} (1 - \kappa_\infty), \quad (30)$$

where

$$\kappa_\infty = \frac{\alpha_\infty}{0.73 + 0.083\sqrt{\alpha_\infty} + \alpha_\infty}. \quad (31)$$

In addition, the fraction of plasma motion which is turbulence,  $\varepsilon = \kappa_{tu}/\kappa_v$ , can be of the order of  $\varepsilon = 0.05$  [25]. Therefore, the dominant source coming from the plasma motion is attributed to the sound waves,  $\kappa_{sw} = (1 - \varepsilon)\kappa_v$ .

Now, by obtaining the key parameters and determining the contribution of each GW source, Eqs. (18), (22) and (23), we compute the GW spectrum generated from

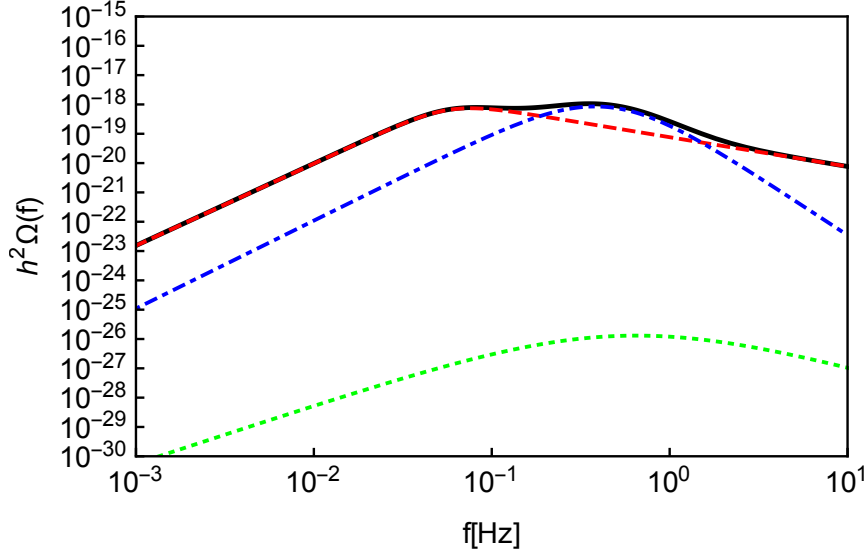


Figure 5: We plot the contribution of each source producing GWs during the EWPT in the presence of the hypermagnetic field  $B_Y^{\text{bg}}/T_*^2 = 0.7$ . The Black solid curve shows the total GW spectrum. The significant contribution belongs to the bubble collision source, the red dashed curve. The blue dotdashed and green dotted curves show the sound wave and MHD turbulence contributions, respectively.

the EWPT and show the results for  $B_Y^{\text{bg}}/T_*^2 = 0.7$  in Fig. (5). As can be seen in Fig. (5), the main contribution comes from the bubble collisions, followed by that of the sound waves. In Fig. (6), we show the GW spectrum for the three values of  $B_Y^{\text{bg}}$  shown in Table 2. As listed in Table 2, larger  $B_Y^{\text{bg}}$  gives rise to greater  $\alpha$  and so stronger first-order EWPT (see Fig. (4)), leading to GWs with higher energy density but lower peak frequency (see Fig. (6)).

As can be seen in Fig. (6), these GWs can be detected by future space-based Ultimate-DECIGO and BBO correlated detectors [17]. Ultimate-DECIGO and BBO correlated are two future-planned interferometers which will be able to detect GWs around 0.1 – 10 Hz at which noises raised from irresolvable gravitational wave signals are negligible [29]. Therefore, these detectors have higher sensitivity and can cover the gap frequency band between LISA and ground-based detectors. Moreover, the interferometers which consist of several detectors can enhance their sensitivity by a few orders of magnitude by making correlation analysis between independent detectors. In fact, Ultimate-DECIGO and BBO correlated interferometers can reach a sensitivity level of the order of  $10^{-20}$  and  $10^{-17}$ , respectively, around 0.1 Hz [18]. Finally, we expect that these GW spectra predicted by our model with peak frequency between 0.1 – 1 Hz can be captured by the most sensitive frequency range of these two detectors, provided  $B_Y^{\text{bg}}$  is large enough.

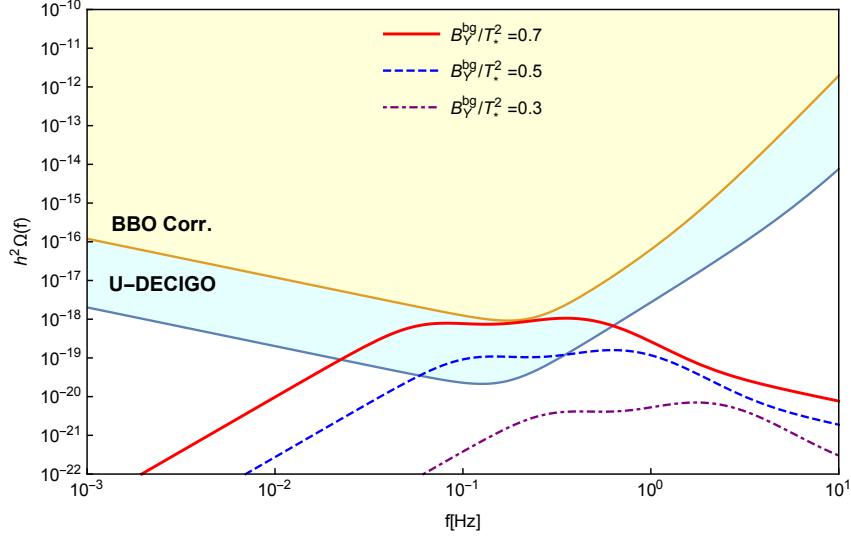


Figure 6: We display the energy density of GWs generated from the first-order EWPT within our model, for the three values of  $B_Y^{\text{bg}}$  shown in Tables 1 and 2. Note that as the value of  $B_Y^{\text{bg}}$  increases, the energy density of GWs increases, while the peak frequency decreases. As can be seen, for large enough  $B_Y^{\text{bg}}$ , these GWs can be in the sensitivity range of the Ultimate-DECIGO (U-DECIGO) and BBO correlated (BBO Corr.) interferometers.

## 4 Conclusion

We have shown that the presence of a large-scale background hypermagnetic field,  $B_Y^{\text{bg}}$ , can have profound effects on the EWPT. In particular, we have shown that as the temperature drops,  $B_Y^{\text{bg}}$  produces a second minimum at a yet larger value of  $\phi$  which eventually becomes the true vacuum. This makes a two-step transition: a crossover to a temporary vacuum followed by a first-order to the final vacuum. The barrier between the two minima also depends on the strength of  $B_Y^{\text{bg}}$ . We have computed all of the important characteristic quantities for the first-order part, including the details of the formation and evolution of bubbles of true vacuum associated with the broken phase, the Higgs profile, the duration of the PT, the latent heat and all of the characteristic temperatures. We find that by enhancing  $B_Y^{\text{bg}}$  the transition temperature is lowered and VEV is increased. We have then explored one of the consequences of the first-order part of EWPT, which is the generation of GWs. We have shown that in our model the bubbles are “runaway”, i.e. the bubble wall speed  $v_b = 1$  and thereby all three sources of GWs, i.e. bubble collisions, sound waves and MHD turbulence contribute. Particularly, we have shown that the bubble collision is the dominated source of the GWs. We have obtained the energy density spectrum of GWs as a function of frequency and shown that their detection is within the range of Ultimate-DECIGO interferometer for  $B_Y^{\text{bg}} \gtrsim 0.5T_*^2$  and BBO correlated interferometer for  $B_Y^{\text{bg}} \gtrsim 0.7T_*^2$ , all for peak frequencies of about 0.1 – 1 Hz.

## Acknowledgments

HA and SSG would like to thank the research council of the Shahid Beheshti University for financial support. MA would like to thank Yasaman Farzan for useful comments. MA is supported by Saramadan grant (c/o M. M. Sheikh-Jabbari) no. ISEF/M/97219.

## References

- [1] A. Neronov and I. Vovk, *Science* **328**, 73 (2010) [arXiv:1006.3504 [astro-ph.HE]].
- [2] A. Brandenburg and K. Subramanian, *Phys. Rept.* **417**, 1 (2005) [astro-ph/0405052].
- [3] M. S. Turner and L. M. Widrow, *Phys. Rev. D* **37**, 2743 (1988); T. Vachaspati, *Phys. Lett. B* **265**, 258 (1991).
- [4] M. Giovannini and M. E. Shaposhnikov, *Phys. Rev. Lett.* **80**, 22 (1998) [hep-ph/9708303]; M. Giovannini, *Phys. Rev. D* **61**, 063502 (2000) [hep-ph/9906241].
- [5] M. Giovannini, *Phys. Rev. D* **92**, no. 12, 121301 (2015) [arXiv:1511.00138 [astro-ph.CO]]; S. Rostam Zadeh and S. S. Gousheh, *Phys. Rev. D* **95**, no. 5, 056001 (2017) [arXiv:1607.00650 [hep-ph]].
- [6] M. Giovannini and M. E. Shaposhnikov, *Phys. Rev. D* **57**, 2186 (1998) [hep-ph/9710234].
- [7] P. Elmfors, K. Enqvist and K. Kainulainen, *Phys. Lett. B* **440**, 269 (1998) [hep-ph/9806403].
- [8] D. Comelli, D. Grasso, M. Pietroni and A. Riotto, *Phys. Lett. B* **458**, 304 (1999) [hep-ph/9903227].
- [9] H. Abedi, M. Ahmadvand and S. S. Gousheh, *Phys. Lett. B* **786**, 35 (2018) [arXiv:1805.10645 [hep-ph]].
- [10] K. Kajantie, M. Laine, J. Peisa, K. Rummukainen and M. E. Shaposhnikov, *Nucl. Phys. B* **544**, 357 (1999) [hep-lat/9809004].
- [11] M. Giovannini, *Phys. Rev. D* **61**, 063004 (2000) [hep-ph/9905358]; M. Giovannini, *Class. Quant. Grav.* **34**, no. 13, 135010 (2017) [arXiv:1702.04293 [gr-qc]].

- [12] A. Ashoorioon and T. Konstandin, JHEP **0907**, 086 (2009) [arXiv:0904.0353 [hep-ph]]; R. G. Cai, M. Sasaki and S. J. Wang, JCAP **1708**, no. 08, 004 (2017) [arXiv:1707.03001 [astro-ph.CO]]; A. Mazumdar and G. White, arXiv:1811.01948 [hep-ph].
- [13] M. Ahmadvand and K. Bitaghsir Fadafan, Phys. Lett. B **772**, 747 (2017) [arXiv:1703.02801 [hep-th]]; M. Ahmadvand and K. Bitaghsir Fadafan, Phys. Lett. B **779**, 1 (2018) [arXiv:1707.05068 [hep-th]].
- [14] A. Kosowsky, M. S. Turner and R. Watkins, Phys. Rev. Lett. **69**, 2026 (1992).
- [15] A. Kosowsky, A. Mack and T. Kahniashvili, Phys. Rev. D **66**, 024030 (2002) [astro-ph/0111483].
- [16] M. Hindmarsh, S. J. Huber, K. Rummukainen and D. J. Weir, Phys. Rev. Lett. **112**, 041301 (2014) [arXiv:1304.2433 [hep-ph]].
- [17] K. Yagi and N. Seto, Phys. Rev. D **83**, 044011 (2011) Erratum: [Phys. Rev. D **95**, no. 10, 109901 (2017)] [arXiv:1101.3940 [astro-ph.CO]].
- [18] A. Cooray, Mod. Phys. Lett. A **20**, 2503 (2005) [astro-ph/0503118].
- [19] K. Kamada and A. J. Long, Phys. Rev. D **94**, no. 12, 123509 (2016) [arXiv:1610.03074 [hep-ph]].
- [20] M. Quiros, hep-ph/9901312.
- [21] A. D. Linde, Phys. Lett. **100B**, 37 (1981); A. D. Linde, Nucl. Phys. B **216**, 421 (1983) Erratum: [Nucl. Phys. B **223**, 544 (1983)].
- [22] A. Masoumi, K. D. Olum and B. Shlaer, JCAP **1701**, no. 01, 051 (2017) [arXiv:1610.06594 [gr-qc]].
- [23] M. Kamionkowski, A. Kosowsky and M. S. Turner, Phys. Rev. D **49**, 2837 (1994) [astro-ph/9310044].
- [24] S. J. Huber and T. Konstandin, JCAP **0809**, 022 (2008) [arXiv:0806.1828 [hep-ph]].
- [25] M. Hindmarsh, S. J. Huber, K. Rummukainen and D. J. Weir, Phys. Rev. D **92**, no. 12, 123009 (2015) [arXiv:1504.03291 [astro-ph.CO]].
- [26] C. Caprini, R. Durrer and G. Servant, JCAP **0912**, 024 (2009) [arXiv:0909.0622 [astro-ph.CO]].
- [27] C. Caprini *et al.*, JCAP **1604**, no. 04, 001 (2016) [arXiv:1512.06239 [astro-ph.CO]].



- [28] J. R. Espinosa, T. Konstandin, J. M. No and G. Servant, JCAP **1006**, 028 (2010) [arXiv:1004.4187 [hep-ph]].
- [29] S. Sato *et al.*, J. Phys. Conf. Ser. **840**, no. 1, 012010 (2017).